ELECTRON TRANSPORT IN FINITE ONE-DIMENSIONAL QUANTUM-DOT ARRAYS

Hongqi Xu[1,2], Zhen-Li Ji[1], and K.-F. Berggren[1]

[1] Department of Physics and Measurement Technology, Linköping University, S-581 83 Linköping, Sweden

[2] Department of Solid State Physics and the Nanometer Consortium, University of Lund, Box 118, S-221 00 Lund, Sweden

(Received 4 August 1992)

A transfer matrix method is formulated for calculating electron transport in a one-dimensional quantum channel having complicated structure and connected to two-dimensional electron reservoirs. The method has been used to calculate conductance in two types of quantum-dot arrays, namely serpentine (double-bend) quantum-dot arrays and quantum-dot arrays with repulsive and square potentials. It is shown that in both a quantum channel with a double-bend dot and a quantum channel with two square and potential-repulsive dots, singlet conductance peaks can appear at energies below the threshold of the lowest subband. These peaks are associated with resonant tunneling via electron quasi-bound states of the systems. It is also shown that in a quantum channel containing an array of the dots, each peak is split into multiple peaks. This is due to the coupling between the corresponding quasi-bound states in the dot array. It is suggested that some recent measurements on a double-bend structure may be interpreted in such terms.

1. Introduction

Recent advances in nanostructure technology have made it possible to define narrow constrictions in a two-dimensional electron gas (2DEG) formed at a semiconductor heterostructure. In tiny structures, such as quantum wires and quantum dots, electron transport is ballistic and the motion of electrons is governed by quantum mechanics rather than classical mechanics. The quantization of the conductance of narrow constrictions first observed by van Wees *et al.* [1] and Wharam *et al.* [2] and the resonant conductance via quasi-bound states in classically unbound systems [3] are just two examples of recent developments in this area.

Here we report on exact quantum-mechanical calculations of electron transport in two types of one-dimensional quantum-dot arrays, namely serpentine quantum-dot arrays and square-like potential-repulsive quantum-dot arrays, embedded in narrow straight channels delimited by hard-wall boundaries. In order to model transport in the ballistic regime, we have assumed that the arrays are finite and the channels are connected with two semi-infinite 2DEGs, which act as source and drain when a potential difference is applied. Further details of the lateral structure of our quantum systems can be found in the insets of the figures presented in this paper. In the calculation we use a transfer matrix method within the effective mass approximation. The method has been formulated by basing all our matrices throughout the quantum channels on one common basis. Thus the method has significant flexibility, i.e., it can be easily used to treat electron transport in quantum channels having very complicated structures in both the longitudinal and the transverse directions.

In a serpentine quantum-dot array, the electrons injected from a 2D-reservoir with energies lower than the height of the embedded rectangular potential barriers are forced through a series of double-bend quantum dots. The effect of the electron interferences due to a double-bend dot on the quantized conductance plateaus was observed by Wu *et al* [4]. In addition, these authors observed also two conductance peaks below the threshold of the first conductance plateau but associated them with resonant tunneling through impurity states in the

0749-6036/92/060237+06 $08.00/0

system [4]. In this paper, we will show that in a channel containing a double-bend quantum dot the conductance peaks corresponding to resonant tunneling via quasi-bound states in the dot can appear at energies below the threshold of the first conductance plateau. We will also show that in a serpentine quantum-dot array, the coupling between quasi-bound states in the double-bend dots will result in the formation of N-fold splitting states where N corresponds to the number of the double-bend dots in the system. In the square-like potential-repulsive quantum-dot arrays two alternative paths have been provided for the electrons between the two sides of each square barrier. Since the potential of the barriers is repulsive we refer to them as anti-dots. The electron quantum dots in these systems are actually located in between the anti-dots. In this paper we will not discuss the so called electrostatic Aharonov-Bohm effect [5]. Thus we will place all the anti-dots along the central line of the straight channel with the hard-wall boundaries. We will show that conductance peaks can appear at energies below the threshold of the first conductance plateau in the quantum channel containing an array of two anti-dots and that each of them will be split into multiple peaks in the quantum channel containing an array of more than two anti-dots.

2. Theoretical Method

In the calculations we use a transfer matrix method formulated by representing the wave functions of the electron states throughout the straight channel in one common basis. The standard transfer matrix method is suitable to treat a quantum system with the electron potential varied along the transfer direction. The use of one common basis throughout the system makes the method suitable also to treat the system having the electron potential varied not only along the transfer direction but also along the transverse direction.

A fundamental step in the transfer matrix method is to divide the quantum system along the transfer direction into a number of strips which are small enough so that the potential in each strip region was a variation only in the transverse direction. This is illustrated in Fig. 1 where the quantum channel has been partitioned along the transfer direction, i.e. the x-direction, into N strips. Let us assume that $\{\Phi_n(y)\}$ are a complete set of orthonormal functions along the transverse y-direction in the interval $|y| \leq w/2$, where w is the width of the straight channel as indicated in Fig. 1. Using this set of functions as our basis we may write the wave functions of electron states in effective mass approximation in strip region i as

$$\Psi^i(x,y) = \sum_n \Phi_n(y) \sum_\alpha d^i_{n\alpha} \left[b^i_\alpha e^{ik^i_\alpha (x-x^i_0)} + c^i_\alpha e^{-ik^i_\alpha (x-x^i_0)} \right] , \quad (1)$$

where the expansion coefficients $d^i_{n\alpha}$ can be obtained by searching for eigenvalues E^i_α from the system

$$\sum_m \left\{ \left(\varepsilon_n - E^i_\alpha \right) \delta_{nm} + \left(\Phi_n(y) | V^i(y) | \Phi_m(y) \right) \right\} d^i_{m\alpha} = 0 , \quad n = 1, 2, 3, \cdots , \quad (2)$$

where $V^i(y)$ is the electron potential in the strip region i. Once equation (2) is solved, the coefficients b^i_α and c^i_α in Eq. (1) are the remaining unknowns in the expansion for the wave function $\Psi^i(x,y)$. Obviously, we have such

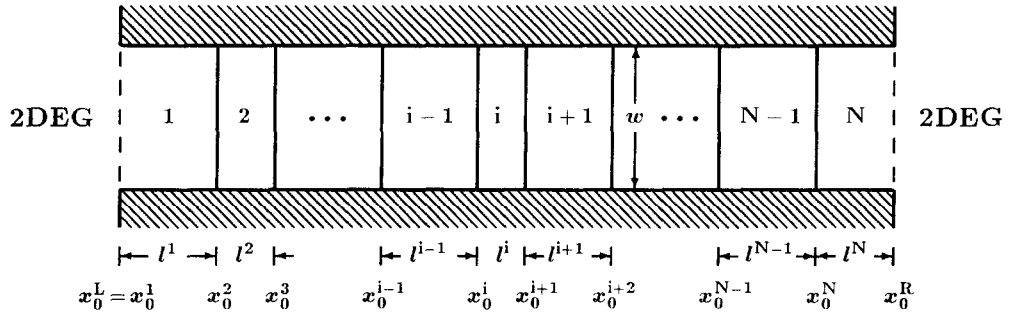

Figure 1: Schematic diagram of a finite quantum channel in which the electron potential varies along both the transportation x- and the transversal y-directions. The channel is connected with two semi-infinite 2DEGs and has been partitioned into N strip regions in such way that in each strip region the electron potential only varies along the transversal y-direction.

a set of coefficients for each strip region. However, the connection between the coefficients of any two strip regions in the channel can be achieved by a transfer matrix in the form

$$\begin{pmatrix} \mathbf{B}^i \\ \mathbf{C}^i \end{pmatrix} = \mathbf{M}(i, i+1) \begin{pmatrix} \mathbf{B}^{i+1} \\ \mathbf{C}^{i+1} \end{pmatrix} , \qquad (3)$$

where $\mathbf{B}^i$ and $\mathbf{C}^i$ are coefficient vectors, whose elements are $\{b^i_\alpha\}$ and $\{c^i_\alpha\}$, respectively, and $\mathbf{M}(i, i+1)$ is the transfer matrix. It can be shown that the transfer matrix $\mathbf{M}(i, i+1)$ is

$$\mathbf{M}(i, i+1) = \begin{pmatrix} \boldsymbol{\gamma}^i & \mathbf{0} \\ \mathbf{0} & (\boldsymbol{\gamma}^i)^{-1} \end{pmatrix}^{-1} \begin{pmatrix} \mathbf{P}^i & \mathbf{P}^i \\ \mathbf{Q}^i & -\mathbf{Q}^i \end{pmatrix}^{-1} \begin{pmatrix} \mathbf{P}^{i+1} & \mathbf{P}^{i+1} \\ \mathbf{Q}^{i+1} & -\mathbf{Q}^{i+1} \end{pmatrix} , \qquad (4)$$

where $\boldsymbol{\gamma}^i$ is the diagonal matrix with elements given by $(\boldsymbol{\gamma}^i)_{\alpha\alpha} = \exp(ik^i_\alpha \ell^i)$, the submatrices $\mathbf{P}^i$ and $\mathbf{Q}^i$ are defined by $(\mathbf{P}^i)_{n\alpha} = d^i_{n\alpha}$ and $(\mathbf{Q}^i)_{n\alpha} = d^i_{n\alpha} k^i_\alpha w$. Here ℓ^i is the width of the ith strip region along the x direction and w is the width of the channel (see Fig. 1). If the channel is divided into N strips, it is straightforward to show that the connection between coefficient vectors at the two end strip regions is

$$\begin{pmatrix} \mathbf{B}^1 \\ \mathbf{C}^1 \end{pmatrix} = \mathbf{M}(1, N) \begin{pmatrix} \mathbf{B}^N \\ \mathbf{C}^N \end{pmatrix} , \qquad (5)$$

where the transfer matrix $\mathbf{M}(1, N)$ is given by

$$\mathbf{M}(1, N) = \mathbf{M}(1, 2)\, \mathbf{M}(2, 3) \cdots \mathbf{M}(N-1, N) . \qquad (6)$$

In order to uniquely determine the coefficient vectors $\mathbf{B}^i$ and $\mathbf{C}^i$ we have to consider the boundary conditions imposed on the two end of the quantum channel. In this work we have connected the channel with two 2DEG-reservoirs and assumed that the electrons are injected from left reservoir and emitted to the right reservoir. By matching the wave functions of the electron states in the channel to the wave functions in the left reservoir, we can derive the boundary conditions imposed on the coefficient vectors $\mathbf{B}^1$ and $\mathbf{C}^1$ in a matrix form as

$$\mathbf{S}(1) \begin{pmatrix} \mathbf{B}^1 \\ \mathbf{C}^1 \end{pmatrix} = \begin{pmatrix} \boldsymbol{\Lambda} \\ \mathbf{0} \end{pmatrix} , \qquad (7)$$

where the vector $\boldsymbol{\Lambda}$ is defined by

$$(\boldsymbol{\Lambda})_n = 2k_x\, w\, \lambda_{nk_y} \qquad (8)$$

with

$$\lambda_{nk_y} = \int_{-\infty}^{\infty} dy\ \Phi^*_n(y)\, \phi^{2D}_{k_y}(y) . \qquad (9)$$

The matrix $\mathbf{S}(1)$ in Eq. (7) is defined by

$$\mathbf{S}(1) \equiv \begin{pmatrix} \mathbf{T}^1_+ & \mathbf{T}^1_- \\ \mathbf{0} & \mathbf{0} \end{pmatrix} , \qquad (10)$$

where $\mathbf{T}^i_+$ and $\mathbf{T}^i_-$ (here i=1) are submatrices with elements given by

$$(\mathbf{T}^i_\pm)_{n\alpha} = \sum_m \left(t_{nm}\, d^i_{m\alpha} \ \pm\ \delta_{nm}\, d^i_{m\alpha}\, k^i_\alpha\right) w \qquad (11)$$

with

$$t_{nm} = \int_{-\infty}^{\infty} dk'_y\ \ k'_x\ \lambda_{nk'_y} \lambda_{k'_y n} . \qquad (12)$$

Similarly, by matching wave functions in the channel to the wave functions in the right reservoir, we can derive the boundary condition imposed on the coefficient vectors $\mathbf{B}^N$ and $\mathbf{C}^N$ as

$$\mathbf{S}(N) \begin{pmatrix} \boldsymbol{\gamma}^N & \mathbf{0} \\ \mathbf{0} & (\boldsymbol{\gamma}^N)^{-1} \end{pmatrix} \begin{pmatrix} \mathbf{B}^N \\ \mathbf{C}^N \end{pmatrix} = \mathbf{0} , \qquad (13)$$

where $\mathbf{S}(N)$ is

$$\mathbf{S}(N) \equiv \begin{pmatrix} \mathbf{0} & \mathbf{0} \\ \mathbf{T}^N_- & \mathbf{T}^N_+ \end{pmatrix} . \qquad (14)$$

We note that for a given channel structure, the matrices $\mathbf{S}(1)$ and $\mathbf{S}(N)$ are energy dependent only, while the vector $\boldsymbol{\Lambda}$ depends on both the energy ε and the direction of the wave vector $\vec{k}$ of the electron in the 2DEG incident on the channel.

Using Eqs. (7) and (13), the coefficient vectors $\mathbf{B}^1$ and $\mathbf{C}^1$ or the coefficient vectors $\mathbf{B}^N$ and $\mathbf{C}^N$ may be eliminated from Eq. (5) and thus the system equation for the expanding coefficients of the wave function in either one of the two end strip regions may be obtained. For example, by eliminating $\mathbf{B}^N$ and $\mathbf{C}^N$, we obtain

$$\left[\, \mathbf{S}(1) \ +\ \mathbf{S}(N)\, \boldsymbol{\Gamma}(N)\, \mathbf{M}^{-1}(1, N) \,\right] \begin{pmatrix} \mathbf{B}^1 \\ \mathbf{C}^1 \end{pmatrix} = \begin{pmatrix} \boldsymbol{\Lambda} \\ \mathbf{0} \end{pmatrix} , \qquad (15)$$

where $\boldsymbol{\Gamma}(N)$ is

$$\boldsymbol{\Gamma}(N) = \begin{pmatrix} \boldsymbol{\gamma}^N & \mathbf{0} \\ \mathbf{0} & (\boldsymbol{\gamma}^N)^{-1} \end{pmatrix} . \qquad (16)$$

Thus the coefficient vectors $\mathbf{B}^1$ and $\mathbf{C}^1$ can simply be obtained by inverting the matrix on the left side of Eq. (15) and all the subsequent coefficient vectors $\mathbf{B}^i$ and $\mathbf{C}^i$, in this example $i = 2, 3, \cdots, N$, can then be computed from them using Eq. (3).

We note that the coefficient vectors and thus the electron wave function in the quantum channel depend on the wave vector $\vec{k}$ of the electron incident on the channel from the left 2DEG reservoir. We may therefore add on the wave function $\Psi(x, y)$ of the electron state a subscript $\vec{k}$ to indicate this dependence explicitly. The electric current carried by the wave function $\Psi_{\vec{k}}(x, y)$ through the quantum channel can simply be expressed in terms of the expansion coefficients of the wave function in any one of the strip regions in the channel. The total current I is then the sum of the contributions form the

electron states $\Psi_{\vec{k}}(x,y)$ of all the incoming wave $\vec{k}$ incident on the channel from the left reservoir in the energy window $(E_F - eV, E_F)$, where E_F is the Fermi energy of the reservoir and V is a potential difference between the two 2DEG reservoirs. The conductance G of the quantum channel is finally calculated from $G = |I/V|$. In the linear response regime, V is assumed to be very small and G is independent of V. For further computational details we refer to Ref. [6].

3. Results and Discussion

The calculations presented in this paper have all been performed with the assumption of an effective mass $m^* = 0.067m_e$ which is appropriate to the $Al_xGa_{1-x}As$/GaAs interface. In most cases (Figures 2–5) we have chosen to plot the calculated conductance G in units of $2e^2/h$ as a function of a dimensionless variable $\xi = (w/\pi\hbar)(2m^*E_F)^{1/2}$, where w is chosed to be the width of the straight quantum channel and E_F is the Fermi energy in the 2DEGs. We have fixed w to a value of 100 nm and varied only the Fermi energy E_F.

We first present our results for the serpentine (i.e. double-bend) quantum-dot structures. We have idealized our quantum systems by implanting rectangular barriers of a finite height V_b in a straight channel of width w delimited by hard walls. The effect of the barrier height V_b on the conductance G of the quantum channels with such serpentine quantum dots can be found in Fig. 2. In this figure we have shown, as an example, the conductance G of the channel with a single double-bend dot (see the inset of the figure for the geometrical detail). The curve with $V_b = 0$ corresponds to the conductance of a pure straight channel of width $w = 100$ nm defined by hard-wall boundaries. The novel plateau structure of a straight channel is clearly seen. Here the oscillations at the edges of the plateaus are due to the presence of longitudinal standing waves in the straight channel because of

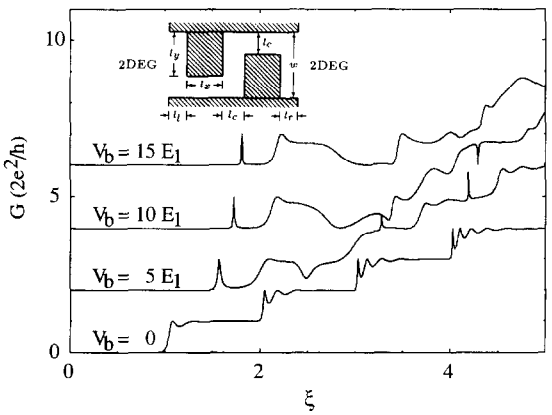

Figure 2: Calculated conductance G as a function of the dimensionless variable $\xi = (w/\hbar\pi)(2m^*E_F)^{1/2}$ for the quantum channel with the single double-bend modulation established by implanting two rectangular barriers of different heights V_b in an otherwise straight quantum channel of width w delimited by hard-wall boundaries. The geometrical detail of the double-bend structure is shown in the inset of this figure with $w = 100$ nm, $l_x = 50$ nm, $l_y = 60$ nm, $l_l = l_r = 30$ nm, and $l_c = w - l_y = 40$ nm. The curves have been offset for clarity.

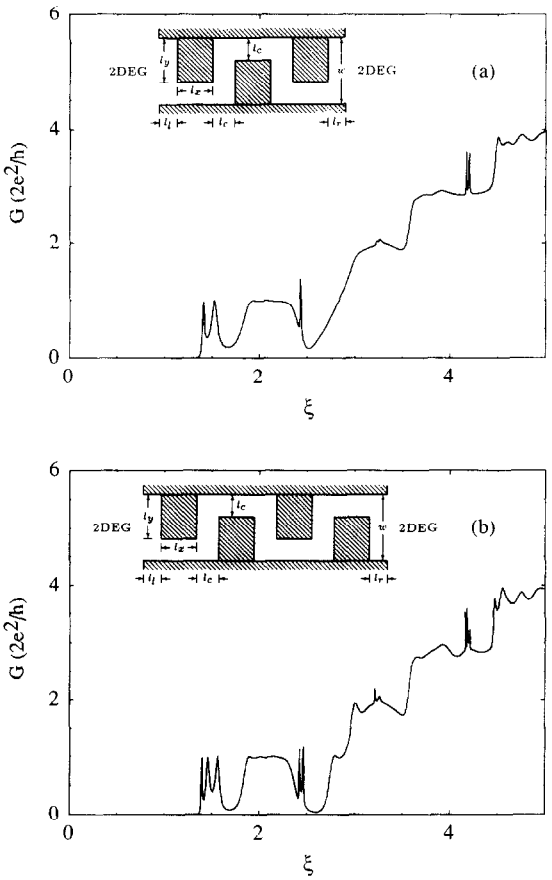

Figure 3: Calculated conductance G as a function of the dimensionless variable $\xi = (w/\hbar\pi)(2m^*E_F)^{1/2}$ for the quantum channels with (a) the double and (b) the triple double-bend modulation established by implanting the rectangular barriers of a fixed height $V_b = 5E_1$ in an otherwise straight quantum channel of width w delimited by hard-wall boundaries. The geometrical details of the two multiple double-bend structures are shown in the insets of the two figures. All other parameters are the same as in Fig. 2.

using sharp corner boundaries at the ends of the channel. As the barrier height V_b is increased, the plateau structure of the straight channel is seen to be disturbed, whereas a sharp conductance peak appears at a energy below the lowest subband threshold E_t [at $V_b \to \infty$, $E_t = (\hbar^2/2m^*)\pi^2/(w - l_y)^2$]. This peak is associated with resonant tunneling via a quasi-bound state localized in the double-bend dot. At $V_b = 15E_1$, where $E_1 = (\hbar^2/2m^*)(\pi/w)^2$ is the first tansversal-mode energy corresponding to the straight channel of width w with hard-wall boundaries, a very broadened peak appears at an energy close to the lowest subband threshold. We have found [6] that at a very high barrier height V_b this peak becomes sharp. The appearance of the peak indicates that there can exist another quasi-bound state at energy below the lowest subband threshold in such a double-bend system at infinite barrier height ($V_b \to \infty$). Thus we propose that the two conductance peaks observed by Wu *et al.* [4] in a double-bend channel at gate voltage below the threshold of the first conductance plateau may be interpreted in terms of resonant tunneling via quasi-bound states. In a quantum-dot array the quasi-bound states discussed above will couple to each other, resulting in multiple-splitting quasi-bound states. As a consequence, multiple-splitting peaks in the conductance may appear at energies below the threshold of the lowest conductance plateau. Fig. 3 shows the calculated conductance for a double and a triple double-bend structures with the same quantum-dot geometry as in the single double-bend structure described in Fig. 2. Here we have set $V_b = 5E_1$, since we are mainly interested in quasi-bound states at energies below the threshold of the first conductance plateau. In a single double-bend quantum-dot system, only one resonant conductance peak appears at energy below the threshold of the first conductance plateau at $V_b = 5E_1$ (see Fig. 2). This peak is seen to be split into two peaks in the double double-bend quantum-dot system and three peaks in the triple double-bend quantum-dot system. Such a multiple-splitting-peak structure in conductance is a typical feature of a finite quantum-dot superlattice [7].

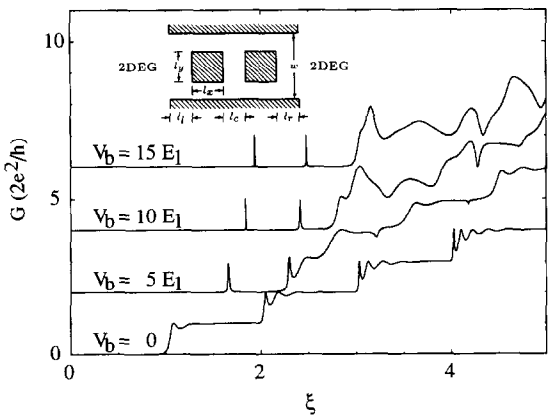

Figure 4: Calculated conductance G as a function of the dimensionless variable $\xi = (w/\hbar\pi)(2m^*E_F)^{1/2}$ for the array of two square-like potential-repulsive barriers of different heights V_b implanted in the center of an otherwise straight quantum channel of width w delimited by hard-wall boundaries. The geometrical detail of the array structure is shown in the inset of this figure with w = 100 nm, $l_x = l_y$ = 50 nm, $l_l = l_r$ = 30 nm, and l_c = 40 nm. The curves have been offset for clarity.

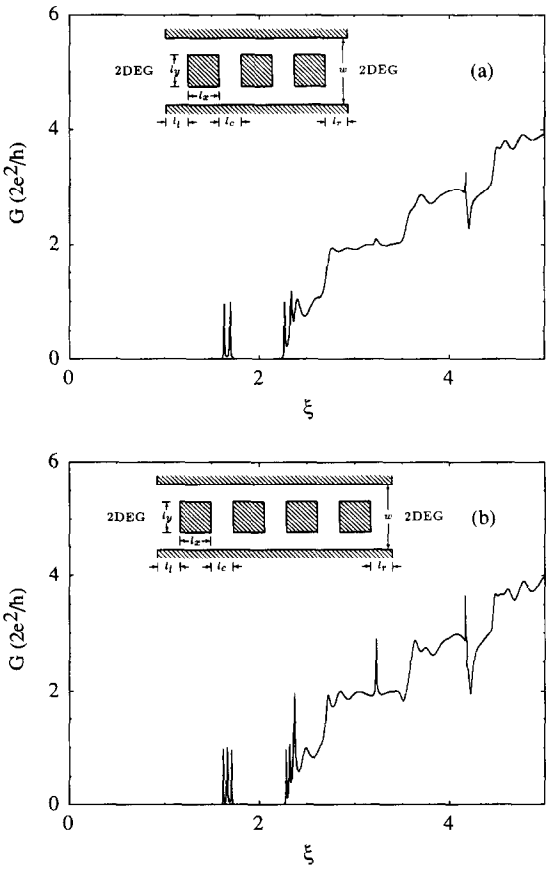

Figure 5: Calculated conductance G as a function of the dimensionless variable $\xi = (w/\hbar\pi)(2m^*E_F)^{1/2}$ for the arrays of (a) three and (b) four square-like potential-repulsive barriers of a fixed height $V_b = 5E_1$ implanted in the center of an otherwise straight quantum channel of width w delimited by hard-wall boundaries. The geometrical details of the two array structures are shown in the insets of the two figures. All other parameters are the same as in Fig. 4.

Our calculated results for the conductance of square-like potential-repulsive quantum-dot arrays implanted in a straight channel of width $w = 100$ nm is shown in Figs. 4–6. Since the potential of the square-like barriers (denoted also by V_b) is repulsive, these barriers are naturally considered as quantum anti-dots. The actual electron quantum dots are located in between the anti-dots. In Fig. 4 we present the calculated conductance G as a function of the dimensionless variable ξ for an array of two square-like barriers of different height V_b. Again, at $V_b = 0$, the calculated curve in this figure corresponds to the conductance of a pure straight channel of width $w = 100$ nm delimited by hard walls. At $V_b \neq 0$, the novel quantized plateau structure is seen to be disturbed and the threshold of the lowest subband is seen to be shifted to a higher value of ξ. Below the up-shifted threshold there are sharp resonant conductance peaks. Here we only see the singlet peaks. This is in correspondence with that there can only appear one electron quantum dot in an array of two square-like anti-dots. Fig. 5 shows the calculated conductance G for an array of three square-like anti-dots and an array of four square-like anti-dots with $V_b = 5E_1$. In a rather similar way to what we see in the calculated conductance for the arrays of the double-bend quantum-dot arrays (Fig. 3), the singlet conductance peak at an energy below the threshold of the lowest conductance plateau in the array of two square-like anti-dots is seen to be split into two (three) peaks in the array of three (four) square-like anti-dots. Such splitting peaks can also be seen at the edge of the lowest conductance plateau. Finally, we wish to present in Fig. 6 the calculated conductance as a function of the Fermi energy E_F for an array of six square-like anti-dots at $V_b = E_1$ and to note that the miniband structure resulting from coupling of quasi-bound states in a quantum-dot array may also appear at conductance plateaus [8-10].

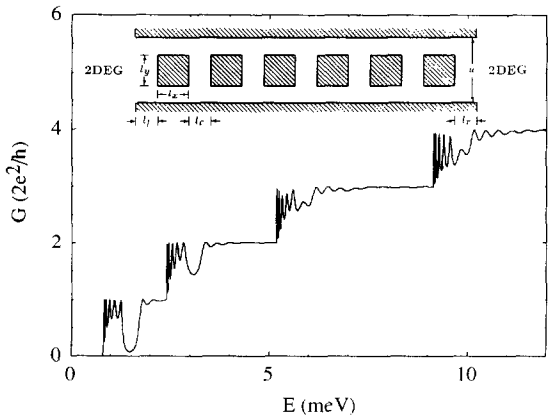

Figure 6: Calculated conductance G as a function of the Fermi energy E_F for the array of six square-like potential-repulsive barriers of a fixed height $V_b = 5E_1$ implanted in the center of an otherwise straight quantum channel of width w delimited by hard-wall boundaries. The geometrical detail of the array structure is shown in the inset of this figure. All other parameters are the same as in Fig. 4.

All results presented so far refer to structures with very sharp features. In a real structure, however, corners tend to be rounded. We have therefore also investigated the case of circular bends. Also in this case there are quasi-bound states below the first subband threshold. As above there are also N-fold splittings for N consecutive double circular bends. The binding energies are, however, much smaller for circular bends. In a real device the situation is in between these two extrme cases.

Acknowledgement – This work has been supported by the Swedish Natural Science Research Council and the Swedish Engineering Research Council.

References

1. B.J. van Wees, H. van Houten, C.W.J. Beenakker, J. G. Williamson, L.P. Kouwenhoven, D. van der Marel, and C.T. Foxon, Phys. Rev. Lett. **60**, 848 (1988).
2. D.A. Wharam, T.J. Thornton, R. Newbury, M. Pepper, H. Ahmed, J.E.F. Frost, D.G. Hasko, D.C. Peacock, D.A. Ritchie, and G.A. Jones, J. Phys. C: Solid State Phys. **21**, L209 (1988).
3. K.-F. Berggren and Zhen-li Ji, Phys. Rev. B **43**, 4760 (1991).
4. J. C. Wu, M. N. Wybourne, W. Yindeepol, A. Weisshaar, and S. M. Goodnick, Appl. Phys. Lett. **59**, 102 (1991).
5. S. Datta, Superlatt. Microstruct. **6**, 83 (1989).
6. Hongqi Xu, to be published.
7. Zhen-Li Ji and K.-F. Berggren, Phys. Rev. B **45**, 6652 (1992) and references cited therein.
8. L.P. Kouwenhoven, F.W.J. Hekking, B.J. van Wees, C.J.P.M. Harmans, C.E. Timmering, and C.T. Foxon, Phys. Rev. Lett. **65**, 361 (1990).
9. S.E. Ulloa, E. Castaño, and G. Kirczenow, Phys. Rev. B **41**, 12350 (1990).
10. Hua Wu, D.W.L. Sprung, J. Martorell, S. Klarsfeld, Phys. Rev. B **44**, 6351 (1992).